J. Iron Steel Res. Int. (2024) 31:1873–1885
https://doi.org/10.1007/s42243-024-01250-1

ORIGINAL PAPER

Effect of slag composition on kinetic behavior of deep deoxidation of 5 wt.% Si high-silicon austenitic stainless steel

Guan-xiong Dou[1,2] · Han-jie Guo[1,2] · Jing Guo[1,2] · Xue-cheng Peng[1,2] · Qing-yun Chen[1,2]

Received: 28 July 2023 / Revised: 5 November 2023 / Accepted: 18 January 2024 / Published online: 9 July 2024

Abstract

Based on a thermodynamic study of 5 wt.% Si high-silicon austenitic stainless steel (SS-5Si) smelting using CaF_2–CaO–Al_2O_3–MgO–SiO_2 slag to obtain a low oxygen content of less than 10×10^{-4} wt.%, a kinetic mass transfer model for deep deoxidation was established through laboratory studies, and the effects of slag components and temperature on deoxidation during the slag–steel reaction process of SS-5Si were systematically studied. The experimental data verified the accuracy of the model predictions. The results showed that the final oxygen content in the steel at 1873 K was mainly controlled by the oxygen content derived from the activity of SiO_2 regulated by the [Si]–[O] equilibrium reaction in the slag system; in particular, when the slag basicity R ($R = w(\mathrm{CaO})/w(\mathrm{SiO_2})$, where w(CaO) and $w(\mathrm{SiO_2})$ are the contents of CaO and SiO_2 in the slag, respectively) is 3, the Al_2O_3 content in the slag needs to be less than 2.7%. The mass transfer rate equation for the kinetics of the deoxidation reaction revealed that the mass transfer of oxygen in the liquid metal is the rate-controlling step under different slag conditions at 1873 K, and the oxygen transfer coefficient $k_{\mathrm{O,m}}$ increases with increasing the slag basicity from 4.0×10^{-6} m s^{-1} ($R = 1$) to 4.3×10^{-5} m s^{-1} ($R = 3$). $k_{\mathrm{O,m}}$ values at $R = 2$ and $R = 3$ are almost the same, indicating that high slag basicity has little effect. The integral of the mass transfer rate equation for the deoxidation reaction of SS-5Si under different slag conditions is obtained. The total oxygen content of the molten steel decreases with increasing basicity from an initial content of 22×10^{-4} to 3.2×10^{-4} wt.% ($R = 3$), consistent with the change in $k_{\mathrm{O,m}}$ with slag basicity. At $R = 2$, the slag–steel reaction takes 15 min to reach equilibrium ($w[\mathrm{O}] = 5.5 \times 10^{-4}$ wt.%), whereas at $R = 3$, the slag–steel reaction takes 30 min to reach equilibrium ($w[\mathrm{O}] = 3.2 \times 10^{-4}$ wt.%). Considering the depth of deoxidation and reaction time of SS-5Si smelting, it is recommended the slag basicity be controlled at approximately 2. Similarly, the effect of temperature on the deep deoxidation of SS-5Si was studied.

Keywords Slag–steel reaction · Kinetics · Rate-controlling step · Deep deoxidation · Transfer coefficient

1 Introduction

High-silicon-containing stainless steels (Si > 4 wt.% in general) possess excellent corrosion resistance in hot concentrated sulfuric acid or concentrated nitric acid, good mechanical properties and low alloy cost and are recognized as a preferred structural material in the sulfuric acid manufacturing industry [1–3]. It is well known that oxygen and sulfur, the two most common harmful elements in the formation of non-metallic inclusions, destroy the continuity of the steel matrix and the uniformity of the structure, seriously affecting the corrosion resistance of stainless steel [4–7], especially the pitting resistance [8] and cracks caused by stress corrosion [9]. Reformatskaya et al. [10] pointed out that the dissolution of inclusions or the adjacent matrix in mild steel is the key to trigger pitting. The effect of oxide and sulfide inclusions in mild steel on corrosion was further investigated by Shibaeva et al. [11]. It was found that oxide inclusions did not affect the active dissolution of mild steel, but changes in passive current values

✉ Han-jie Guo
guohanjie@ustb.edu.cn

✉ Jing Guo
guojing@ustb.edu.cn

[1] School of Metallurgical and Ecological Engineering, University of Science and Technology Beijing (USTB), Beijing 100083, China

[2] Beijing Key Laboratory of Special Melting and Preparation of High-End Metal Materials, Beijing 100083, China

and breakdown potentials were correlated with the inclusion content. Sulfide inclusions lead to an increase in corrosion current, and the higher the sulfur content, the weaker the passivation of the steel and the narrower the range of passive potentials. Researchers have come to a consensus that the lower the contents of harmful oxygen and sulfur in steel are, the more corrosion resistant the steel will be. Some researchers selected several manganese steels with different oxygen contents (w[O] = 44 × 10^{-4}–150 × 10^{-4} wt.%) and conducted kinetic potential polarization experiments in 3 wt.% NaCl solution at pH of 10. It was found that the steel with a lower deoxidation content (44 × 10^{-4} wt.%) exhibited enhanced pitting resistance [12]. Ismail and Adan [13] compared the corrosion performance of AISI 1040 steel with a high oxygen content and an ultra-low oxygen content less than 10 × 10^{-4} wt.% in H_2SO_4 solution, and the results showed that the corrosion rate of the ultra-low-oxygen steel was 0.0034 mm/a, and that of the high-oxygen content steel was 0.364 mm/a, which represented a huge improvement in the corrosion resistance. Li et al. [14] designed six sets of electrochemical experiments on 316L stainless steel with different oxygen contents in a simulated proton exchange membrane fuel cell (PEMFC) cathodic environment, and the results showed that 316L stainless steel with an oxygen content of 10 × 10^{-4} wt.% had the best corrosion resistance and that the thickness of the passivation film and the Cr_2O_3 content increased with the reduction in oxygen content in the cathodic environment.

Slag refining is integral to the processes of deoxidation and desulfurization, as well as the absorption and eradication of inclusions, thereby serving as an efficacious measure for assessing and regulating the steel cleanliness [15–19]. Lei et al. [20] have demonstrated that by refining the chemical composition of Al_2O_3–CaO–SiO_2–MgO slag, one can modulate the deformability of inclusions and the contents of oxygen, sulfur, and aluminum, thus achieving a high degree of purity in spring steel. Yan et al. [21] investigated the desulfurization of stainless steel with an initial sulfur content of 150 × 10^{-4} wt.% using CaO–SiO_2–CaF_2 (CSF)-type slag and a series of CaO–Al_2O_3 (CA)-type slags. The cleanliness of steels with a low final sulfur content (30 × 10^{-4}–50 × 10^{-4} wt.%) was improved, with a reduced number density, size, and fractional area of sulfide inclusions. The refining process of Al-killed steel usually uses CaO–SiO_2–Al_2O_3-type slag with MgO to prevent excessive corrosion of the MgO(–C)-type ladle lining [22–24]. Wang et al. [25] found that an Al_2O_3 content of less than 8 wt.% in slag is favorable for obtaining inclusions with lower melting points. To obtain the optimum inclusion composition with a low melting point, the optimum refining slag basicity should be determined. Durinck et al. [26] found that when the slag basicity (R = w(CaO)/w(SiO_2), where w(CaO) and w(SiO_2) are the contents of CaO and SiO_2 in the slag, respectively) exceeds 4, increasing the basicity does not improve the purity of bearing steel. Adjusting the ratio of w(CaO)/w(Al_2O_3) (where w(Al_2O_3) is the content of Al_2O_3 in the slag) is the most effective way to remove inclusions. It has been verified that when the slag basicity is determined to be 4, the optimal w(CaO)/w(Al_2O_3) ratio is approximately 1.7. Yan et al. [21] conducted desulfurization experiments on austenitic stainless steels with CA-type slags in the interval of 1873–1923 K. It was found that the rate of desulfurization increased with increasing w(CaO)/w(Al_2O_3), and a desulfurization kinetic model based on the double-film theory was developed. Studies on the thermodynamics and kinetics of the associated slag-steel reaction are relatively rare.

There are few basic studies on the deep removal of oxygen and sulfur to less than 10 × 10^{-4} wt.% in 5 wt.% Si high-silicon austenitic stainless steel (SS-5Si), and the authors have carried out a study on the deep removal of oxygen in this stainless steel to less than 10 × 10^{-4} wt.% based on thermodynamics and laboratory experiments [27]. However, studies on the deep removal of oxygen and sulfur in steel to less than 10 × 10^{-4} wt.% on the basis of the kinetics of the slag–steel reaction by using the optimized slag system are still rare. It can be expected that when the oxygen and sulfur contents in the SS-5Si are less than 10 × 10^{-4} wt.%, its high-temperature corrosion resistance will be satisfactory.

To solve the above problems, in this study, based on the thermodynamic study of deep deoxidation of SS-Si [27], we explore the kinetics of deep deoxidation using CaF_2–CaO–Al_2O_3–MgO–SiO_2 slag system. The aim is to determine the rate-controlling step of the reaction under the condition of removing oxygen and sulfur to approximately 5 × 10^{-4} wt.% and to establish a kinetic mass transfer rate model for the deep removal of oxygen and sulfur, providing a theoretical basis for large-scale production.

2 Experimental design and procedure for assessing deep deoxidation kinetics of SS-5Si

2.1 Thermodynamic considerations

To investigate the kinetics of deep deoxidation of SS-5Si, it is first necessary to clarify whether the ultra-low oxygen content of less than 5 × 10^{-4} wt.% in the steel during refining is thermodynamically controlled by the equilibrium of the deoxidation reaction of [Si]–[O] or [Al]–[O] for the following two reactions:

$$[\mathrm{Si}] + 2[\mathrm{O}] = (\mathrm{SiO_2}) \tag{1}$$

$$\lg K_{\mathrm{Si}} = \lg \frac{a_{\mathrm{SiO_2}}}{a_{[\mathrm{Si}]} a_{[\mathrm{O}]}^2} = \lg \frac{a_{\mathrm{SiO_2}}}{f_{\mathrm{Si}} w[\mathrm{Si}] f_{\mathrm{O}}^2 w[\mathrm{O}]^2} = \frac{30,110}{T} - 11.4 \tag{2}$$

$$[\mathrm{Al}] + 1.5[\mathrm{O}] = (\mathrm{AlO_{1.5}}) \tag{3}$$

$$\lg K_{\mathrm{Al}} = \lg \frac{a_{\mathrm{AlO_{1.5}}}}{a_{[\mathrm{Al}]} a_{[\mathrm{O}]}^{1.5}} = \lg \frac{a_{\mathrm{AlO_{1.5}}}}{f_{\mathrm{Al}} w[\mathrm{Al}] f_{\mathrm{O}}^{1.5} w[\mathrm{O}]^{1.5}} = \frac{32,000}{T} - 10.29 \tag{4}$$

where K_i is the reaction equilibrium constant for the oxidation reaction of element $[i]$ in molten steel; $a_{[i]}$ and f_i are the activity and activity coefficient of component i in a metal relative to the 1% standard state, with the mass percentage $w[i]$ as the concentration unit; a_i is the activity of component i in the slag relative to pure matter as a standard state, with the mole fraction x_i as the concentration unit; and T is temperature.

The final dissolved oxygen content in the steel (i.e., the deoxidation limit) is related to the [Si]–[O] equilibrium and the [Al]–[O] equilibrium. The oxygen content in steel that is in equilibrium with SiO_2 and Al_2O_3 in the slag is expressed as $w[\mathrm{O}]_{\mathrm{Si}}$ and $w[\mathrm{O}]_{\mathrm{Al}}$, respectively. Based on Eqs. (1)–(4), the relationship between the equilibrium oxygen content in sulfuric acid-resistant stainless steel during refining and variables such as the activity a_i of component i in the CaF_2–CaO–Al_2O_3–MgO–SiO_2 slag, the chemical composition of SS-5Si and the reaction temperature could be obtained by simple mathematical derivation, as shown in Eqs. (5) and (6).

$$\lg w[\mathrm{O}]_{\mathrm{Si}} = \frac{1}{2}\left\{\lg a_{\mathrm{SiO_2}} - \lg f_{\mathrm{Si}} - 2\lg f_{\mathrm{O}} - \lg w[\mathrm{Si}] - \left(\frac{34,458}{T} - 11.96\right)\right\} \tag{5}$$

$$\lg w[\mathrm{O}]_{\mathrm{Al}} = \frac{2}{3}\left\{\lg a_{\mathrm{AlO_{1.5}}} - \lg f_{\mathrm{Al}} - 1.5\lg f_{\mathrm{O}} - \lg w[\mathrm{Al}] - \left(\frac{32,000}{T} - 10.29\right)\right\} \tag{6}$$

From Eqs. (5) and (6), it can be seen that the parameters needed to calculate the equilibrium oxygen content of the liquid steel are (1) the activity of the relevant components in the slag ($a_{\mathrm{SiO_2}}, a_{\mathrm{AlO_{1.5}}}$), which can be calculated using the ion–molecule coexistence theory (IMCT) model [28], and (2) the activity coefficients for Si, Al and O at different reaction temperatures, which were calculated by the Wagner equation [29] for the chemical compositions of SS-5Si shown in Table 1. The relevant activity interaction coefficients used are shown in Table 2.

The oxygen control mechanism of the reaction of SS-5Si with CaF_2–CaO–Al_2O_3–MgO–SiO_2 slag at 1873 K was obtained in our previous study [27]. It was determined that the equilibrium oxygen content was determined by the greater of two factors: $w[\mathrm{O}]_{\mathrm{Si}}$ and $w[\mathrm{O}]_{\mathrm{Al}}$.

To obtain a more accurate picture of the slag components when $w[\mathrm{O}]_{\mathrm{Si}}$ determines the equilibrium oxygen content in steel, the thermodynamic prediction model was used to calculate the effect of Al_2O_3 content (1–10 wt.%) on $w[\mathrm{O}]_{\mathrm{Si}}$ and $w[\mathrm{O}]_{\mathrm{Al}}$ in slag containing w(MgO) = 10 wt.% and $w(CaF_2)$ = 20 wt.% with binary basicities of 1, 2 and 3 as shown in Fig. 1. The results show that both $w[\mathrm{O}]_{\mathrm{Si}}$ (solid line) and $w[\mathrm{O}]_{\mathrm{Al}}$ (dashed line) calculated by the thermodynamic model decrease with increasing the slag basicity at 1873 K, and they can be reduced below 5×10^{-4} wt.% at R = 3. The measured values are in good agreement with the calculated values, where $w[\mathrm{O}]_{\mathrm{Si}} \geq$ TO (total oxygen) > $w[\mathrm{O}]_{\mathrm{Al}}$, indicating that the equilibrium oxygen content of the liquid steel is controlled by the [Si]–[O] equilibrium reaction under the abovementioned slag composition.

In particular, when R = 3, the dashed line and solid line will intersect at the point M (2.72, 2.89) as $w(Al_2O_3)$ gradually increases. The coordinates of point M correspond to $w(Al_2O_3)$ = 2.72% in the slag and an equilibrium oxygen content value of 2.89×10^{-4} wt.%. In this case, the equilibrium oxygen content in the steel depends on the [Si]–[O] reaction when $w(Al_2O_3) < 2.72\%$ and R = 3. Conversely, when $w(Al_2O_3) > 2.72\%$ and R = 3, the equilibrium oxygen content in the steel depends on the [Al]–[O] reaction. However, when R = 3, the oxygen control mechanism will change with increasing the Al_2O_3 content in the slag. To keep the equilibrium oxygen content in steel less than 2.89×10^{-4} wt.% and ensure that the [Si]–[O] equilibrium reaction is the oxygen-controlling reaction, it is sufficient to control $w(Al_2O_3)$ within 2.72%.

Therefore, the [Si]–[O] reaction is the sole reaction to be considered in the study of kinetics section, rather than the [Al]–[O] reaction. It also provides a range for slag design in the following kinetic experiments.

2.2 Experimental materials and methods

The SS-5Si was fabricated by vacuum induction melting process using MgO crucibles, and the chemical composition is listed in Table 1. The starting melting vacuum is 1.0×10^{-2}–2.0×10^{-2} Pa, and a high vacuum is always maintained during the melting period. During casting, the steel is remelted at 1485–1495 °C based on cooling remelting. Table 3 shows the composition of the slag. The effects of basicity on oxygen content can be compared using S1, S2, and S3. The effects of Al_2O_3 content on oxygen content can be compared using S4, S5, and S6. The effects of CaF_2 content on oxygen content can be compared

Table 1 Chemical components of molten metal used in present study (wt.%)

C	Si	Mn	Al	Mo	Cr	Ni	Cu	O	S	N	Fe
0.02	5	0.49	0.1	1.13	12.95	18.3	1.05	0.0025	0.0022	0.01	Balance

Table 2 Interaction coefficients e_i^j used in present study [28]

e_i^j	C	Si	Mn	Al	Mo	Ni	Cr	O	S
O	− 0.45	− 0.131	− 0.021	− 3.9	0.0035	0.008	− 0.04	− 0.2	− 0.133
Si	0.18	0.11	0.002	0.058	–	0.005	–	− 0.23	0.056
Al	0.091	0.0056	–	0.045	–	–	–	6.60	0.03
S	0.11	0.063	− 0.026	0.035	0.002	0	− 0.01	− 0.27	− 0.028

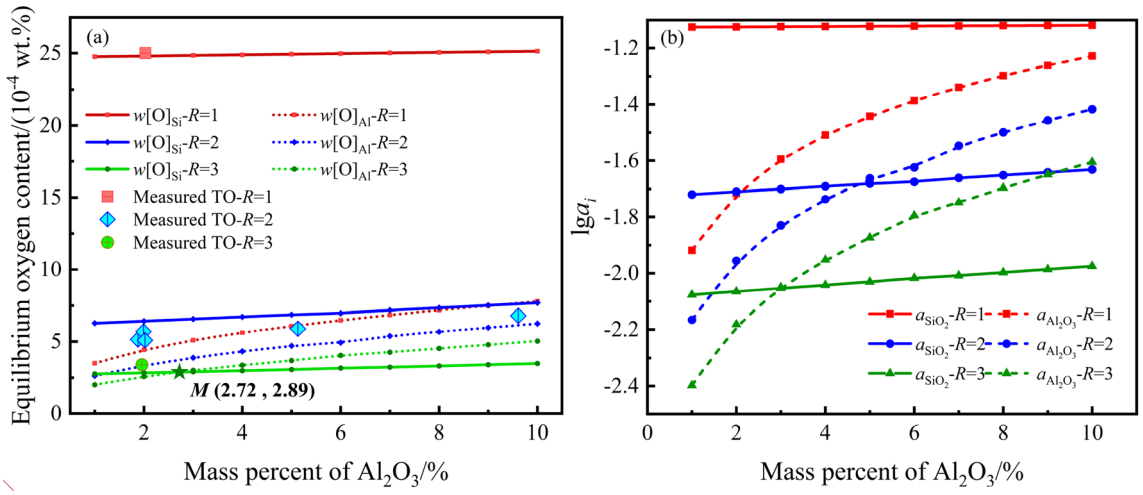

Fig. 1 Relationship between basicity and Al_2O_3 content in CaF_2–CaO–Al_2O_3–MgO–SiO_2 slag for equilibrium oxygen content (**a**) and a_{SiO_2} and $a_{Al_2O_3}$ at 1873 K for a certain steel composition (**b**)

Table 3 Composition of slag used in this study (wt.%)

Slag No.	CaO	SiO_2	CaF_2	MgO	Al_2O_3
S1	29.44	29.44	29.31	9.83	1.98
S2	38.35	19.17	30.27	10.19	2.02
S3	44.53	14.84	29.23	9.60	1.80
S4	38.80	18.21	30.63	10.31	2.04
S5	37.13	18.56	29.31	9.87	5.13
S6	34.59	17.29	28.70	10.06	9.61
S7	44.73	22.37	20.87	10.04	1.99
S8	42.21	21.11	25.33	9.47	1.88
S9	38.64	18.14	31.23	10.08	1.91

using S7, S8, and S9. The slag contained sufficient magnesium oxide to prevent erosion of the magnesium oxide crucible.

The experiments were conducted in a vertical resistance heated aluminum tube furnace utilizing $MoSi_2$ as heating elements. A schematic diagram of the resistance furnace

used in this study is shown in Fig. 2 and the operational steps in the smelting experiments are illustrated in Fig. 3. To control the temperature of the heating furnace, a proportional–integral–derivative (PID) controller was coupled to a type B reference thermocouple. In preparation for the experiment, another type B thermocouple was used to calibrate the temperature to 1873 K. The experimental steps are as follows:

(1) The slag was prepared in a graphite crucible (OD: 50 mm, ID: 44 mm, H: 88 mm), and then, the graphite crucible was placed in an electric resistance furnace under a purified Ar atmosphere and positioned in the constant-temperature zone. The furnace was heated from room temperature to 1873 K and kept at 1873 K for 20 min to ensure that the sample had a uniform composition.

(2) The pre-melted slag (10 g) was held in the upper graphite crucible with a small hole in its bottom. An inner wall angle of 110° ensured that the melted slag fell into the lower crucible. The graphite plug in the hole was used to control the reaction time of slag and steel. After polishing the test steel (40 g), it was placed in a MgO crucible (OD: 30 mm, ID: 25 mm, H: 35 mm). To prevent MgO crucible rupture, the outer layer of the MgO crucible was covered with a graphite crucible (OD: 36 mm, ID: 31 mm, H: 40 mm). A large graphite crucible (OD: 66 mm, ID: 54 mm, H: 140 mm) was placed outside the double-layer crucible to make it easier to handle.

(3) After the temperature reached 1873 K, the double-layer crucible was placed in an electric resistance furnace under a purified Ar atmosphere (2–4 L/min), and the temperature was decreased. When the temperature recovered to 1873 K, it was kept at this value for 15 min to ensure that the steel and slag were completely melted. At the moment, the graphite plug was removed, and the reaction between slag and steel began. This time was taken as the starting time for the reaction.

(4) After certain reaction time intervals (1, 5, 10, 15 and 30 min), the whole crucible was rapidly removed from the furnace and placed in a bucket with ice water. After the completion of the reaction between slag and steel, a sample of about 1 g steel was removed from the reaction products to analyze the content of total oxygen by an oxygen, nitrogen and hydrogen analyzer (TCH600, LECO, USA). The sulfur content in the steel samples was analyzed using a carbon–sulfur analyzer (ELTRA CS-3000) at the National Analysis Center for Iron and Steel (NACIS), China. At least three samples of metal were taken to analyze the composition in each test run, and the average of the three results was used as the oxygen content in the ingot.

3 Kinetic modeling of deep deoxidation reaction

Under the slag conditions where the thermodynamic [Si]–[O] equilibrium reaction controls the equilibrium oxygen content in the liquid steel, a kinetic mass transfer model of the [Si]–[O] reaction was developed to study the rate-controlling step (RCS) of the deoxidation reaction based on the measured values of TO for the deep deoxidation reaction under nine different slag compositions, as shown in Tables 3 and 4.

$$[\mathrm{Si}] + [\mathrm{O}] = (\mathrm{SiO_2}) \tag{7}$$

Based on the boundary layer theory defined by Wagner [30], the mechanism of reaction (7) between slag and steel may be divided into the following four elementary steps:

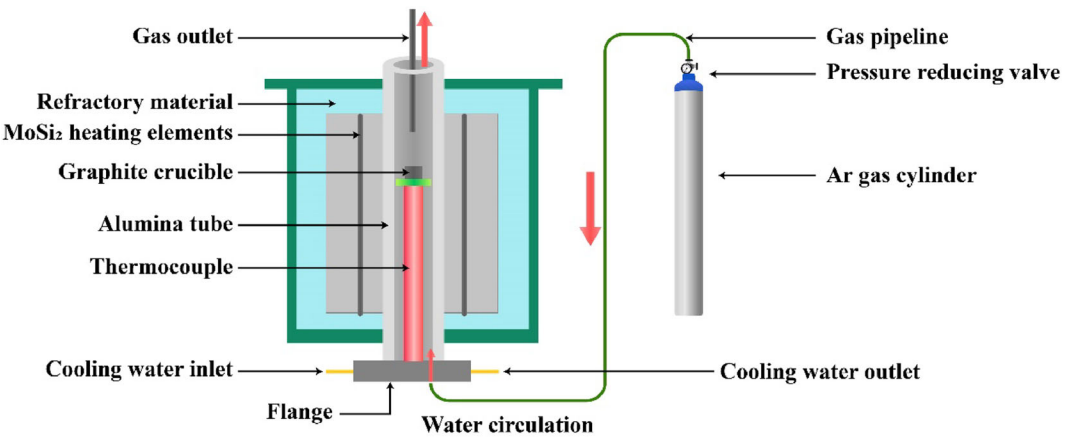

Fig. 2 Schematic of experimental equipment used

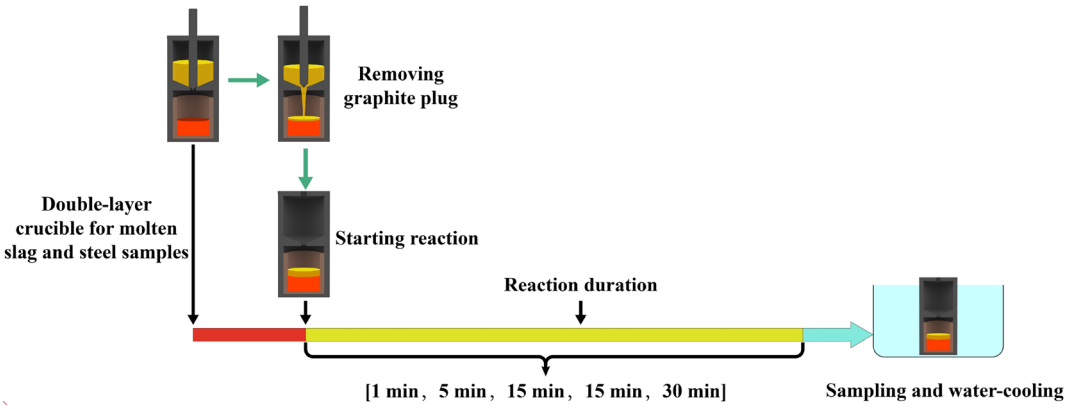

Fig. 3 Flow sheet of experimental procedure

Table 4 Total oxygen content of experimental ingots at 1873 K (wt.%)

Slag No.	0 min	1 min	5 min	10 min	15 min	30 min
S1	22.0×10^{-4}	23.0×10^{-4}	23.8×10^{-4}	24.4×10^{-4}	24.8×10^{-4}	25.0×10^{-4}
S2	22.0×10^{-4}	17.8×10^{-4}	10.5×10^{-4}	7.9×10^{-4}	6.3×10^{-4}	5.5×10^{-4}
S3	22.0×10^{-4}	16.4×10^{-4}	8.5×10^{-4}	5.1×10^{-4}	3.5×10^{-4}	3.2×10^{-4}
S4	22.0×10^{-4}	17.5×10^{-4}	11.5×10^{-4}	8.1×10^{-4}	7.2×10^{-4}	6.5×10^{-4}
S5	22.0×10^{-4}	18.7×10^{-4}	13.4×10^{-4}	9.0×10^{-4}	8.0×10^{-4}	7.6×10^{-4}
S6	22.0×10^{-4}	19.4×10^{-4}	14.1×10^{-4}	9.5×10^{-4}	8.8×10^{-4}	8.1×10^{-4}
S7	22.0×10^{-4}	16.7×10^{-4}	11.0×10^{-4}	8.1×10^{-4}	7.1×10^{-4}	6.5×10^{-4}
S8	22.0×10^{-4}	16.5×10^{-4}	10.5×10^{-4}	7.9×10^{-4}	6.9×10^{-4}	6.3×10^{-4}
S9	22.0×10^{-4}	16.2×10^{-4}	9.8×10^{-4}	7.6×10^{-4}	6.5×10^{-4}	5.9×10^{-4}

(1) Mass transfer of [Si] in the molten steel from the bulk to the slag–metal interface: $[Si] \rightarrow [Si]^*$;
(2) Mass transfer of [O] in the molten steel from the bulk to the slag–metal interface: $[O] \rightarrow [O]^*$;
(3) Interface chemical reaction: $[Si]^* + 2[O]^* = (SiO_2^*)$;
(4) Mass transfer of the generated SiO_2 from the slag–steel interface to the slag phase: $(SiO_2)^* \rightarrow (SiO_2)$.

It is widely accepted that interfacial chemical reaction rates at high temperatures are fast and step (3) will not be the RCS in the reaction kinetics [31]. Steps (1), (2) or (4) corresponding to the mass transfer of reactants or products through the concentration boundary layer into or out of the slag–metal interface are likely to be the RCS of the reaction at high temperatures.

According to the fundamental equation of heterogeneous reaction kinetics based on the concept of the effective boundary layer [32], the flux of component i (i = [Si], [O], and (SiO_2)) across unit area J is defined according to Eq. (8).

$$J_i = \frac{1}{A}\frac{\mathrm{d}n_i}{\mathrm{d}t} = k_{i,\mathrm{s}}\left(C_{i,\mathrm{s}}^{*} - C_{i,\mathrm{s}}^{\mathrm{b}}\right) = k_{i,\mathrm{m}}\left(C_{i,\mathrm{m}}^{\mathrm{b}} - C_{i,\mathrm{m}}^{*}\right) \tag{8}$$

where J_i is the molar flow, mol m^{-2} s^{-1}; $k_{i,\mathrm{m}}$ and $k_{i,\mathrm{s}}$ represent the mass transfer coefficients of element i in the steel melt and slag component i, respectively, m^{-1}, while subscripts 's' and 'm' indicate the slag and metal phase, respectively; n_i is the amount of substance of element i in molten steel and components in slag; C_i is their molar concentration by volume, mol m^{-3}; t is the reaction time; A is the slag–metal interfacial areas; and superscripts '*' and 'b' represent the interface and bulk phase respectively.

For reaction (7), the following relationship holds between the reaction rates expressed by [Si] and [O] in the liquid steel and (SiO_2) in the slag:

$$-\frac{1}{2}\frac{\mathrm{d}n_{[\mathrm{O}]}}{\mathrm{d}t} = -\frac{\mathrm{d}n_{[\mathrm{Si}]}}{\mathrm{d}t} = \frac{\mathrm{d}n_{(\mathrm{SiO_2})}}{\mathrm{d}t} \tag{9}$$

On the basis of the relationship between volumetric molar concentration and mass fraction: $C_i = \frac{w[i]}{100}\frac{\rho_{\mathrm{m}}}{M_i}$. Herein, ρ_{m} is the density of the molten steel, g cm^{-3}; and M_i represents the molar mass of element i in the molten steel, g mol^{-1}. This relationship is also defined by the volume molar concentration equation $C_i = \frac{n_i}{V}$, where V represents

the volume of the molten steel, cm^3. By substituting the two equations into Eq. (8), Eq. (10) can be derived.

$$\frac{dw[i]}{dt} = \frac{A\rho_m k_i}{W_m}\left(w[i]^* - w[i]^b\right) \tag{10}$$

where W_m represents the mass of the molten steel, g. For the [Si]–[O] reaction, the reaction rate is expressed as:

$$\frac{dw[O]}{dt} = \frac{A\rho_m k_{O,m}}{W_m}\left(w[O]^* - w[O]^b\right) \tag{11}$$

The relationship between $\frac{dw[O]}{dt}$, $\frac{dw[Si]}{dt}$ and $\frac{dw(SiO_2)}{dt}$ can be obtained from Eq. (9)

$$\frac{dw[Si]}{dt} = \frac{1}{2}\frac{M_{Si}}{M_O}\frac{dw[O]}{dt}, \frac{dw(SiO_2)}{dt} = -\frac{1}{2}\frac{W_m}{W_s}\frac{M_{SiO_2}}{M_O}\frac{dw[O]}{dt} \tag{12}$$

Suppose $Q_{SiO_2} = \left[\frac{1}{2}\cdot\frac{W_m}{W_s}\cdot\frac{M_{SiO_2}}{M_O}\right] = 7.51$, $Q_{Si} = \left[\frac{1}{2}\frac{M_{Si}}{M_O}\right] = 0.875$, and then,

$$\frac{dw[Si]}{dt} = Q_{Si}\frac{dw[O]}{dt}, \frac{dw(SiO_2)}{dt} = -Q_{SiO_2}\frac{dw[O]}{dt} \tag{13}$$

where W_s represents the mass of the slag, g.

The maximum rate of oxygen mass transfer in steel can be deduced from Eq. (11). The concentration of oxygen at the slag–steel interface can be calculated from the mass action law, which should be satisfied by the activity of each substance in Eq. (7) when the interfacial chemical reaction reaches equilibrium, i.e.,

$$K_{Si} = \frac{a_{SiO_2}}{a_{[O]}^2 a_{[Si]}} = \frac{\gamma_{SiO_2}x^*_{SiO_2}}{f_O^2 w[O]^2 f_{Si} w[Si]} \tag{14}$$

where γ_i is the activity coefficient of component i in the slag relative to pure matter as a standard state.

The relationship between the molar fraction of a slag component and its mass can be expressed by $x_i = \frac{n_i}{\sum n_i} = \frac{m_i}{M_i\sum n_i}$, where $\sum n_i$ is the total mole number in 100 g slag, mol; and m_i is the mass of the component corresponding to the slag.

Since the mass of the initial slag is assumed to be 100 g in the modeling calculations of IMCT,

$$x_i = \frac{w(i)}{M_i\sum n_i} \tag{15}$$

Since the compositions of the components (e.g., Si, O and SiO_2) in reaction (7) do not change much, the activity coefficients of the above components can be approximated as constants during the reaction. By combining these constants $\frac{f_O^2 f_{Si} M_{SiO_2}\sum n_i}{\gamma_{SiO_2}}$ with the chemical equilibrium constant K_{Si}, the effective equilibrium constant E_{Si} can be expressed as follows:

$$E_{Si} = \frac{w(SiO_2)^*}{w[O]^{*2}w[Si]^*} = K_{Si}\cdot\frac{f_O^2 f_{Si} M_{SiO_2}\sum n_i}{\gamma_{SiO_2}} \tag{16}$$

From Eq. (16), the concentration of oxygen at the interface is given as follows:

$$w[O]^* = \sqrt{\frac{w(SiO_2)^*}{E_{Si}w[Si]^*}} \tag{17}$$

Assuming that the mass transfer of [O] in the liquid steel is the RCS, as shown in Fig. 4, then $w(SiO_2)^* = w(SiO_2)$ and $w(Si)^* = w(Si)$. By substituting Eq. (17) into Eq. (11), the following equation can be obtained:

$$-\frac{dw[O]}{dt} = -\frac{A\rho_m k_{O,m}}{W_m}\left[\sqrt{\frac{w(SiO_2)^*}{E_{Si}w[Si]^*}} - w[O]^b\right] \tag{18}$$

or

$$-\frac{dw[O]}{dt} = \frac{A\rho_m k_{O,m}}{W_m}\left[w[O]^b - \sqrt{\frac{w(SiO_2)^*}{E_{Si}w[Si]^*}}\right] \tag{19}$$

The equation for the rate of deoxidation of [O] in the liquid steel where the mass transfer is the RCS can be obtained as

$$\left(-\frac{dw[O]}{dt}\right) = \frac{A\rho_m k_{O,m}}{W_m}\left[w[O]^b - \sqrt{\frac{w(SiO_2)^b}{E_{Si}w[Si]^b}}\right] \tag{20}$$

$w(SiO_2)^b$ and $w[Si]^b$ in Eq. (20) are closely related to the changes of oxygen content in molten steel. This is because the [Si]–[O] reaction requires the consumption of 1/2 mol of [Si] for every 1 mol of [O] removed while producing 1/2 mol of SiO_2. According to the principle of mass conservation, it is assumed that the initial oxygen content during the reaction in the steel is $w[O]^0$ and the oxygen content in the bulk metal at time t is $w[O]$. Then, the change in the oxygen content of the molten steel is

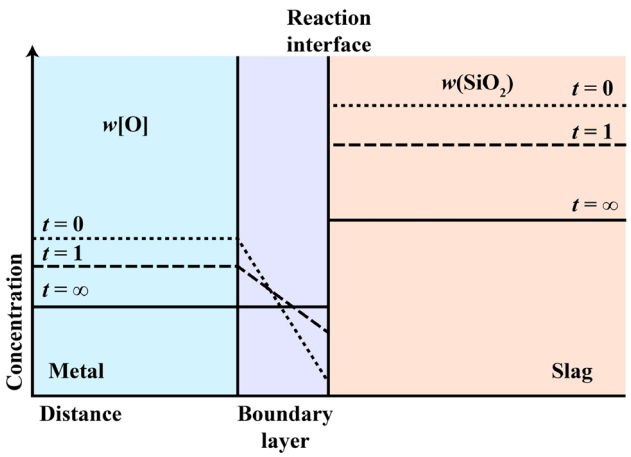

Fig. 4 Schematic diagram of [O] mass transfer as RCS in liquid steel

$\Delta w[\mathrm{O}] = w[\mathrm{O}] - w[\mathrm{O}]^0$. The SiO_2 content of the slag will increase $Q_{SiO_2} w[\mathrm{O}]$ at time t. The SiO_2 content in the bulk slag at time t is:

$$w(SiO_2) = w(SiO_2)^0 - Q_{SiO_2}\Delta w[\mathrm{O}] \tag{21}$$

Similarly, the Si content in the liquid steel at time t is:

$$w[\mathrm{Si}] = w[\mathrm{Si}]^0 + Q_{\mathrm{Si}}\Delta w[\mathrm{O}] \tag{22}$$

Substituting Eqs. (21) and (22) into Eq. (20) results in the following equation:

$$\left(\frac{\mathrm{d}w[\mathrm{O}]}{\mathrm{d}t}\right) = \frac{A\rho_{\mathrm{m}}k_{\mathrm{O,m}}}{W_{\mathrm{m}}}\left[\sqrt{\frac{w(SiO_2)^0 - Q_{SiO_2}\Delta w[\mathrm{O}]}{E_{\mathrm{Si}}\left(w[\mathrm{Si}]^0 + Q_{\mathrm{Si}}\Delta w[\mathrm{O}]\right)}} - w[\mathrm{O}]\right]. \tag{23}$$

Form Eq. (23), the variables can be separated, and integration yields Eq. (24):

$$\int_{w[\mathrm{O}]^0}^{w[\mathrm{O}]} \frac{\mathrm{d}w[\mathrm{O}]}{\sqrt{\frac{w(SiO_2)^0 - Q_{SiO_2}\Delta w[\mathrm{O}]}{E_{\mathrm{Si}}\left(w[\mathrm{Si}]^0 + Q_{\mathrm{Si}}\Delta w[\mathrm{O}]\right)}} - w[\mathrm{O}]} = \frac{A\rho_{\mathrm{m}}k_{\mathrm{O,m}}}{W_{\mathrm{m}}}t \tag{24}$$

Based on a similar approach, the corresponding rate equations assuming that the mass transfer of SiO_2 in the slag and the mass transfer of Si in the molten steel are the RCS can be derived.

For the mass transfer of (SiO_2) in the slag phase as the RCS,

$$\frac{\mathrm{d}w(SiO_2)}{\mathrm{d}t} = -\frac{Q_{SiO_2}\mathrm{d}w[\mathrm{O}]}{\mathrm{d}t} = \frac{A\rho_{\mathrm{s}}k_{SiO_2,\mathrm{s}}}{W_{\mathrm{s}}} \times \left[E_{\mathrm{Si}}w[\mathrm{O}]^2\left(w[\mathrm{Si}^0] + Q_{\mathrm{Si}}\Delta w[\mathrm{O}]\right) - \left(w(SiO_2)^0 - Q_{SiO_2}\Delta w[\mathrm{O}]\right)\right] \tag{25}$$

$$\int_{w[\mathrm{O}]^0}^{w[\mathrm{O}]} Q_{SiO_2}\mathrm{d}w[\mathrm{O}] \Big/ \left[\left(w(SiO_2)^0 - Q_{SiO_2}\Delta w[\mathrm{O}]\right) - E_{\mathrm{Si}} \cdot w[\mathrm{O}]^2 \cdot \left(w[\mathrm{Si}]^0 + Q_{\mathrm{Si}}\Delta w[\mathrm{O}]\right)\right] = \frac{A\rho_{\mathrm{s}}k_{SiO_2,\mathrm{s}}}{W_{\mathrm{s}}}t \tag{26}$$

For the mass transfer of [Si] in the molten steel phase as the RCS,

$$\frac{\mathrm{d}w[\mathrm{Si}]}{\mathrm{d}t} = Q_{\mathrm{Si}}\frac{\mathrm{d}w[\mathrm{O}]}{\mathrm{d}t} = \frac{A\rho_{\mathrm{m}}k_{\mathrm{Si,m}}}{W_{\mathrm{m}}}\left[\frac{w(SiO_2)^0 - Q_{SiO_2}\Delta w[\mathrm{O}]}{E_{\mathrm{Si}} \cdot w[\mathrm{O}]^2} - \left(w[\mathrm{Si}]^0 + Q_{\mathrm{Si}}w[\mathrm{O}]\right)\right] \tag{27}$$

$$\int_{w[\mathrm{O}]^0}^{w[\mathrm{O}]} Q_{\mathrm{Si}}\mathrm{d}w[\mathrm{O}] \Big/ \left[\frac{w(SiO_2)^0 - Q_{SiO_2}\Delta w[\mathrm{O}]}{E_{\mathrm{Si}}w[\mathrm{O}]^2} - \left(w[\mathrm{Si}]^0 + Q_{\mathrm{Si}}\Delta w[\mathrm{O}]\right)\right] = \frac{A\rho_{\mathrm{m}}k_{\mathrm{Si,m}}}{W_{\mathrm{m}}}t \tag{28}$$

Equations (24), (26) and (28) can all be expressed as a function of w[O], and the general formula can be expressed as

$$F(w[\mathrm{O}]) = S_i t \tag{29}$$

When it is assumed that the mass transfer of O or Si in the liquid steel or SiO_2 in the slag is the RCS, the corresponding mass transfer rate model can be assumed to meet Eq. (29), and the curve of $F(w[\mathrm{O}])$ versus time should be a straight line; i.e., the slope S_i is a constant. In this case, it is considered that the assumption that one of the above three mass transfer steps is the RCS is valid, and the corresponding mass transfer coefficients can be obtained from S_i.

4 Experimental results and discussion

4.1 Determination of RCS in kinetics of silicon deoxidation reaction

Because the mass transfer rate model can predict the changes in w[O], slag systems (S1–S3) with the most significant impact on w[O] were selected to determine the RCS of the deoxidation reaction kinetics. The contents of CaF_2 and MgO in the slag systems were basically the same, while $w(Al_2O_3)$ is less than 2.72%. The experimental results of the reactions (shown in Table 4) of slags S1–S3 and SS-5Si (shown in Table 1) at 1873 K were inserted into Eqs. (24), (26) and (28), resulting in Fig. 5. The results show that the slopes of the $F(w[\mathrm{O}])-t$ relationship curves obtained under the assumption that the mass transfer of [Si] in the liquid steel and the mass transfer of (SiO_2) in the slag are the RCSs of the reaction kinetics are almost zero, indicating that these steps are not the RCS of the [Si]–[O] reaction. When assuming that the mass transfer of [O] in the molten steel is the RCS, the slopes of the $F(w[\mathrm{O}])$–t relationship curves for slags S1 (R = 1), S2 (R = 2) and S3 (R = 3) are constant, being 0.00034, 0.00337 and 0.0037, respectively. Therefore, it can be determined that the mass transfer of [O] in the molten steel is the RCS in the Si deoxidation reaction. It can be found from Eq. (24) that S_{O}, as the parameter on the right side of the definite integral sign with respect to variable t, can be expressed by Eq. (30).

$$S_{\mathrm{O}} = \frac{A\rho_{\mathrm{m}}k_{\mathrm{O,m}}}{W_{\mathrm{m}}} \tag{30}$$

Under the condition of a defined steel composition, $k_{\mathrm{O,m}}$ and S_{O} are positively correlated. $k_{\mathrm{O,m}}$ calculated for different basicity levels are shown in Table 5. Among these parameters, the equilibrium content of each component can be derived from thermodynamic equilibrium calculations. The density of the molten steel and molten slag can be determined from the results of previous studies, and the reaction area can be obtained by calculating the diameter of

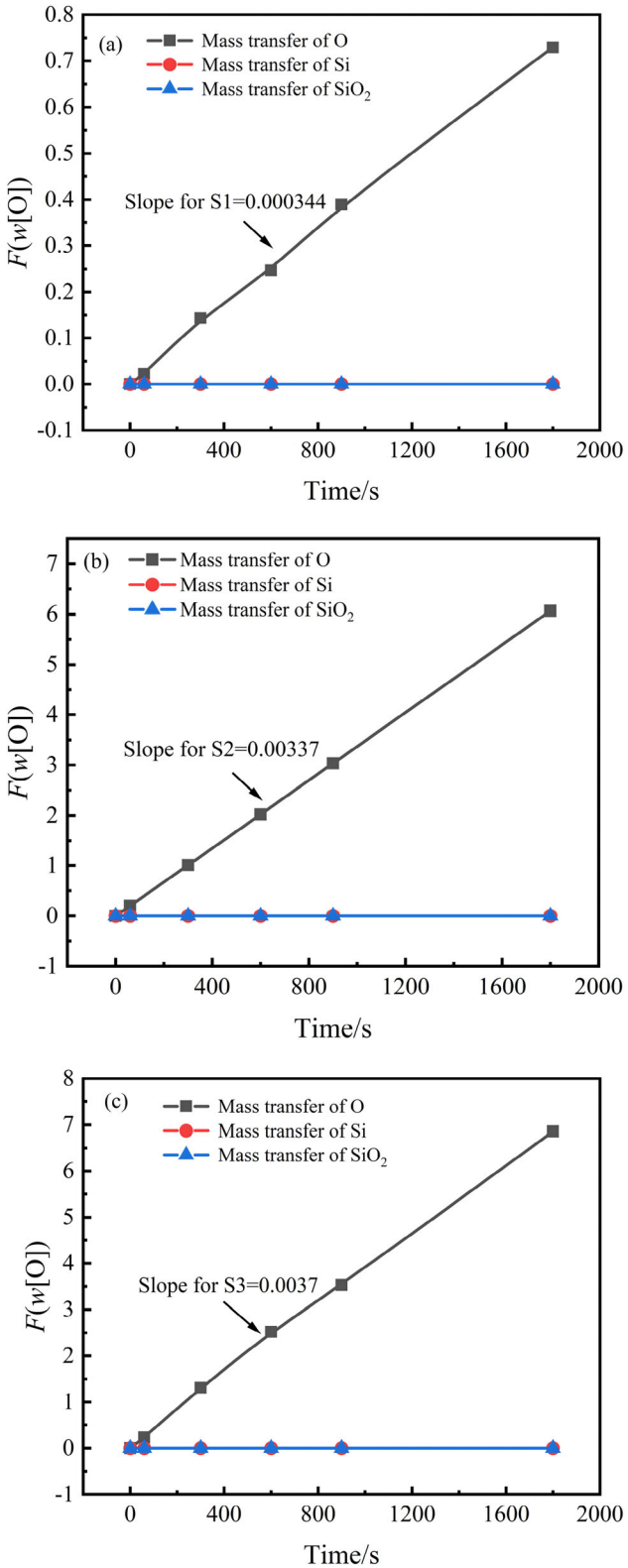

Fig. 5 Oxygen content in liquid metal as a function of reaction time for various slag compositions at 1873 K. **a** S1; **b** S2; **c** S3

the reaction crucible. Some studies [33–36] indicated that the mass transfer coefficient of a component is not fixed under different reaction conditions. For example, k_O of the slag–steel reaction of Si–Mn-killed steel (w[Si] = 0.2 wt.%, w[Mn] = 1.05 wt.%) with CaO–Al_2O_3–MgO–SiO_2-type slag at 1823 K yielded a value of 8×10^{-6} m/s [33]. Shin et al. [34] utilized the effective equilibrium nuclear reaction model to experimentally validate the kinetics of the reaction of Fe–0.8Mn–0.4Si–0.3C–0.05Al steel (mass%) with 40CaO–27Al_2O_3–13SiO_2–10CaF_2–10MgO (mass%) at 1873 K and obtained a value of 1×10^{-4} m/s for k_O. Ren et al. [35] developed a kinetic model for inclusion evolution during the reoxidation process of Al–Ti-containing steels with CaO–Al_2O_3–MgO–SiO_2 slag, and the model was validated using the experimental data of Park et al. [36], obtaining a value of 1×10^{-5} m/s for k_O. It can be noted that the actual value of the mass transfer coefficient varies with the smelted steel grade, slag, heating conditions and other experimental conditions (1×10^{-4}–1×10^{-6} m/s), and it is necessary to validate the mass transfer coefficient of [O] in high-silica stainless steel.

$k_{O,m}$ in steel for CaF_2–CaO–Al_2O_3–MgO–SiO_2 slag at different basicity levels was empirically calculated to be 4.0×10^{-6} m s^{-1} (R = 1), 3.9×10^{-5} m s^{-1} (R = 2), and 4.3×10^{-5} m s^{-1} (R = 3). From a kinetic point of view, as the slag basicity increases, $k_{O,m}$ in steel becomes larger, the mass transfer rate becomes faster, and the oxygen in the steel is more easily removed, which is consistent with the results of thermodynamic calculations. From this perspective, it can also be shown that the corresponding mass transfer coefficients of [Si] in the liquid steel and (SiO_2) in the slag have no effect on the deoxidation rate, which is in agreement with the conclusions of Li et al. [37].

4.2 Influence of slag composition on oxygen content and deoxidation rate in steel

After the [O] mass transfer in the molten steel was identified as the RCS of the [Si]–[O] reaction, the oxygen content in the molten steel at the equilibrium of the slag–steel reaction determined from the thermodynamic study to be the end point of the deoxidation kinetics was compared

Table 5 Value of mass transfer coefficient of [O] and S_O for different slag compositions at 1873 K

R	S_O	A/m^2	W_m/g	$k_{O,m}$/(m s^{-1})
1	0.000344	0.0004906	40	4.0×10^{-6}
2	0.00337	0.0004906	40	3.9×10^{-5}
3	0.0037	0.0004906	40	4.3×10^{-5}

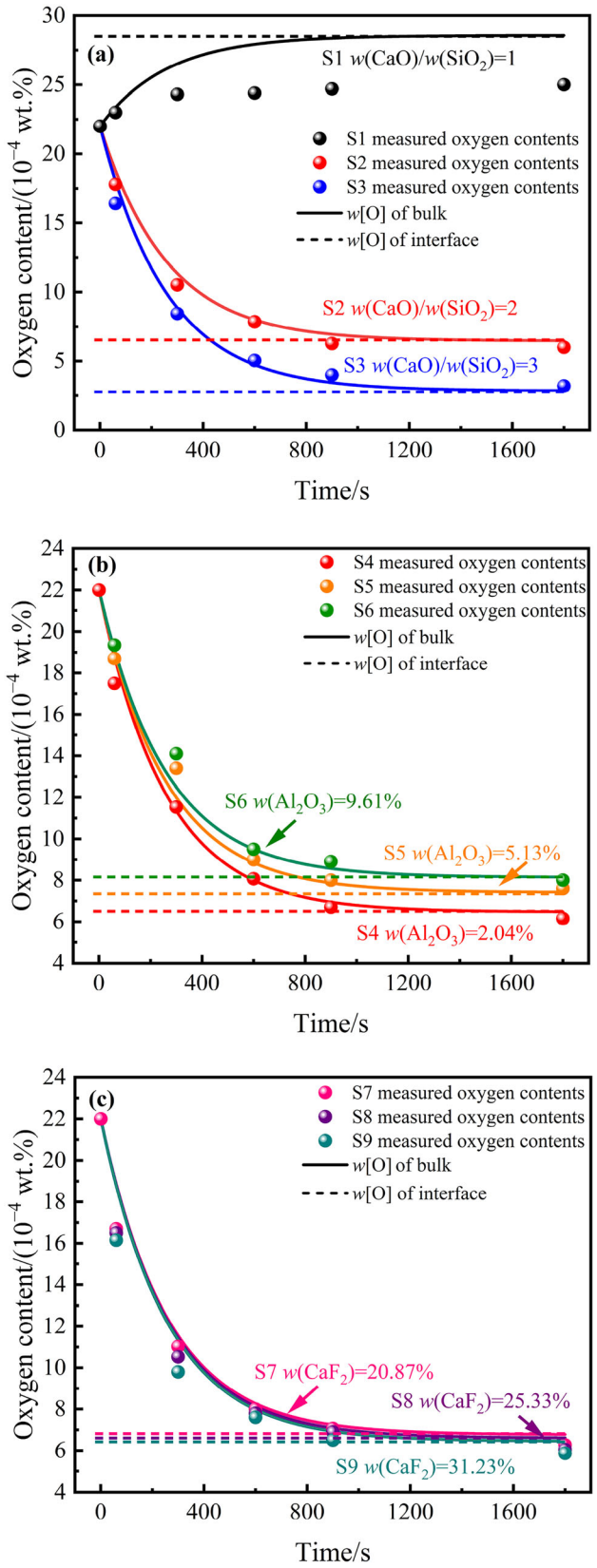

Fig. 6 Model predictions (lines) and experimental data (points) of change in oxygen content with time for different slag compositions at 1873 K. **a** R; **b** Al_2O_3; **c** CaF_2

with the kinetic modeling results. The values indicated how far the slag–steel deoxidation reaction is from the end point of the slag–steel reaction of SS–5Si at a certain temperature. Figure 6 shows the predicted values (solid lines) and experimental results (solid dots) of the obtained kinetic model (Eq. (24) for the time-dependent change in oxygen content in the steel for different slag compositions at 1873 K, as well as the results of the thermodynamic study (dashed lines).

The solid and dashed lines calculated from the developed mass transfer model indicate the internal and interfacial concentrations, respectively, as shown in Fig. 6a. At 1873 K, the equilibrium oxygen content in steel calculated by the kinetic prediction model decreases with increasing the basicity of the CaF_2–CaO–Al_2O_3–MgO–SiO_2 slag. The basic principle behind this result is that increasing the slag basicity induces a decrease in a_{SiO_2}, as shown in Eq. (5), enhancing the deoxidation of silicon in the steel, which agrees with the findings reported by Suito and Inoue [38], Okuyama et al. [39], Ren et al. [40], Wang et al. [41], and others. The results of three laboratory-scale experiments at different basicity levels at 1873 K are also shown in Fig. 6a; the end-point oxygen content in the molten steel was varied from 22.0×10^{-4} wt.% to approximately 25.0×10^{-4}, 5.5×10^{-4}, and 3.2×10^{-4} wt.%, for binary basicity values of the slag system $R = 1$ (S1), $R = 2$ (S2), and $R = 3$ (S3), respectively. Notably, at the slag basicity of 1, the measured oxygen content in the liquid steel increased from 22.0×10^{-4} to 25.0×10^{-4} wt.% (30 min) during the slag–steel reaction. a_{SiO_2} values of the CaF_2–CaO–Al_2O_3–MgO–SiO_2 slag at basicity of 1 and 2 were 0.01341 and 0.00042, respectively, with a difference of two orders of magnitude. The variation caused the $w[O]_{Si}$ of the slag system with a basicity of 1, which was controlled by the [Si]–[O] equilibrium, to be much larger than that for the basicity of 2, followed by that of SS-5Si at 1873 K. The slag–steel reaction at basicity of 1 appears to increase oxygen, which reflects the nature of the slag–steel reaction. Duan et al. [42] also proposed that when the activity of SiO_2 in the slag is low, using Si as a deoxidizer results in an elevated presence of Al_2O_3 and MgO in the deoxidized byproducts, thereby augmenting the oxygen content in steel. This suggests that a more acidic slag composition is detrimental to the deoxidation process.

The effect of basicity on the rate of the deoxidation reaction can be found. When the basicity is 1, the deoxidation reaction reaches the end point after the reaction time of 5 min. After 5 min, the oxygen content in the liquid steel is basically unchanged, indicating that the deoxidation reaction takes 5 min to reach equilibrium with a basicity of 1. When $R = 2$, the slag–steel reaction reaches an equilibrium in 15 min. However, when $R = 3$, the slag–steel

reaction requires 30 min to reach equilibrium. This indicates that as the slag basicity increases, the terminal oxygen content in the steel decreases, and the time required to reach the terminal oxygen content increases nonlinearly. The reason for this may be that when R is 3, the molten steel is very viscous and does not flow well. According to the classical shrinking core reaction models, where the mass transfer of O in the metal is used as the RCS of the reaction and the diffusion coefficients are estimated using the Stokes–Einstein relationship, the total dissolution time (τ) [43] is approximately

$$\tau = \frac{\rho \cdot R_0^2 \cdot 3\pi a\eta}{2kT\Delta C} \tag{31}$$

where ρ is the particle density; R_0 is the radius of the inclusion; ΔC is the driving force for dissolution; k is the Boltzmann constant; a is the ionic diameter; and η is the viscosity of the slag.

For a given temperature and inclusion particle size,

$$\tau \approx \frac{\rho a\eta}{\Delta C} \tag{32}$$

This means that the total dissolution time of oxide inclusions is proportional to the $\eta/\Delta C$ ratio. For SS-5Si, assuming a certain SiO_2 content in the inclusions, the decrease in ΔC caused by the high basicity of the slag increases the viscosity at the same time, thus increasing the total dissolution time. A study by Park et al. [44] also noted that the dissolution of inclusions and the viscosity of the slag directly affect the removal rate of inclusions through the slag and flux layers. Considering the kinetic conditions, at 1873 K, the slag with basicity of 2 needs to react for 15 min to remove the oxygen content in the liquid steel to 5.5×10^{-4} wt.%, while the slag with basicity of 3 needs to react for 30 min to remove the oxygen content in the liquid steel to 3.2×10^{-4} wt.%, which achieve oxygen removal from SS-5Si to 5×10^{-4} wt.% or even below but doubling the smelting time and doubling the cost are not necessary. Therefore, in designing the composition of CaF_2–CaO–Al_2O_3–MgO–SiO_2-type slag, excessive basicity should be avoided, and it is better to adjust the slag basicity at approximately 2.

Figure 6b compares the calculated and measured oxygen contents in CaF_2–CaO–Al_2O_3–MgO–SiO_2 slag at 1873 K with different Al_2O_3 contents. It can be seen that the oxygen content of the steel became larger with increasing the Al_2O_3 content in the slag, and the trend is consistent with the simulation results. As expected, the measured total oxygen content was smaller than the calculated oxygen content. Schneider et al. [45] conducted laboratory remelting tests on bearing steels and found that lowering the Al_2O_3 content in the slag reduces the oxygen content of the steel, which in turn reduces the number of non-metallic inclusions. The influence of Al_2O_3 on the viscosity of high basicity CaO–SiO_2–Al_2O_3–8% MgO–8% CaF_2 slag (w(CaO)/w(SiO_2) = 6) for HRASS Sanicro 25 was systematically investigated by Zhang et al. [46]. As the Al_2O_3 concentration increases from 10% to 25%, the addition of Al_2O_3 predominantly inhibits the precipitation behavior of solid phases, thereby playing a central role in diminishing the viscosity of the slag. With a further increase in Al_2O_3 content to 30%, the facilitating effect of Al_2O_3 on the polymerization degree of the networks becomes the principal contributor to the enhancement of slag viscosity. Chen et al. [47] investigated the quantitative relationship between viscosity and structure within a CaO–SiO_2–MgO–Al_2O_3 slag system with a basicity of 1, uncovering that as the content of Al_2O_3 increased, the viscosity of the slag initially rose and then declined, and unequivocally indicating that Al_2O_3 exerts an amphoteric effect on the viscosity of the slag. Owing to this characteristic property of Al_2O_3, it is imperative to regulate its concentration meticulously, not only to achieve a reduction in slag viscosity but also to fulfill the thermodynamic requirements for lowering the oxygen content. The effect of Al_2O_3 content in slag on the rate of deoxidation reaction can be seen. When $w(Al_2O_3)$ = 2.04%, the deoxidation reaction reaches equilibrium after a reaction time of 15 min. With the increase in Al_2O_3 content to 5.13% and 9.61%, the deoxidation reaction did not reach equilibrium within 15 min. From the kinetic conditions, an increasing Al_2O_3 content affects the mass transfer rate of oxygen in the steel. The results showed that although the change in Al_2O_3 content did not cause a significant change of TO, precise control of the Al_2O_3 content in the slag is required to achieve optimal deoxidation.

The calculated and measured oxygen contents in 1873 K CaF_2–CaO–Al_2O_3–MgO–SiO_2 slag with different CaF_2 contents with time are given in Fig. 6c. The dependence of the oxygen content in the steel on the CaF_2 content in the slag is weak, and the measured results are consistent with the simulation. Zheng et al. [48] investigated the effect of CaF_2 content on high basicity CaO–18% Al_2O_3–SiO_2–10% MgO–CaF_2 (w(CaO)/w(SiO_2) = 6) refining slag suitable for duplex stainless steel. It was shown that the addition of CaF_2 significantly reduced the slag viscosity. However, this effect became less evident with increasing temperature and CaF_2 content. When the CaF_2 content exceeded 10%, the slag viscosity decreased only slightly with the increase in the CaF_2 content. The viscosity of slag containing 6% CaF_2 was very close above 1833 K, while the viscosity below 1833 K is much lower than that of CaO–30% Al_2O_3–SiO_2–10% MgO (w(CaO)/w(SiO_2) = 6) slag without CaF_2. Further evaluation of the effect of 6% CaF_2-containing slag on steel purity confirmed that 6% CaF_2 is sufficient for high basicity slag containing CaF_2. In

light of recent studies reporting that the observed effect can be explained by the evaporation of fluoride from the slag, the remaining fluoride has no significant effect on the change in total oxygen content [49, 50]. The above results show that the established kinetic mass transfer model for the maximum deoxidation rate is suitable for studying the deoxidation behavior of refining slag systems with SS-5Si at different basicities, Al_2O_3 contents, and CaF_2 contents. For a given smelting temperature, the effect of slag components on deoxidation rate follows the order $R > Al_2O_3 > CaF_2$.

4.3 Effect of temperature on rate of deoxidation

The measured oxygen content of steel with respect to time for slag S2 and different smelting temperatures (1673–1873 K) are shown in Table 6 The effect of temperature on the deoxidation of SS-5Si under the action of S2 slag was obtained by substituting the data in Table 6 into Eq. (24), as shown in Fig. 7. With slag S2, the actual equilibrium oxygen content of the steel increased from 2.6×10^{-4} wt.% (1773 K) to 5.5×10^{-4} wt.% (1873 K) with increasing the temperature; i.e., the lower temperature was favorable for deoxidation. When the reaction time was 15 min, the [Si]–[O] reactions all reached equilibrium, which shows that the temperature mainly changed the thermodynamic chemical equilibrium constant of silicon deoxidation and did not have a significant effect on the kinetic conditions.

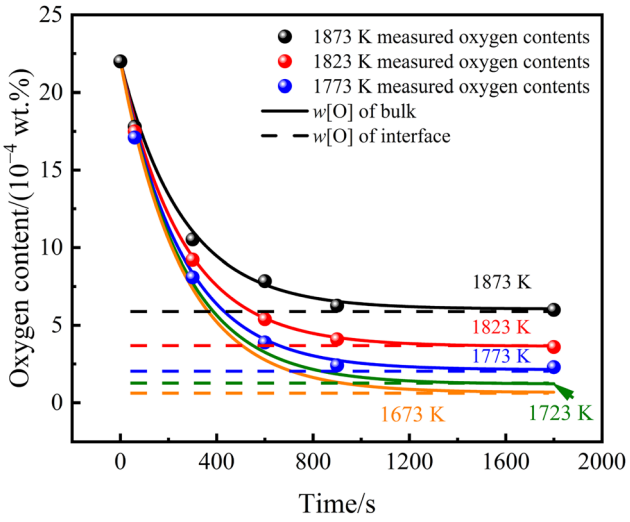

Fig. 7 Effect of temperature on SS-5Si deoxidation rate under slagging of S2

5 Conclusions

1. According to the thermodynamics of the deoxidation behavior of CaF_2–CaO–Al_2O_3–MgO–SiO_2 slag in SS-5Si, the slag fractions that control the equilibrium oxygen content at an ultra-low value of less than 5×10^{-4} wt.% due to the equilibrium of the [Si]–[O] reaction during the refining process were obtained, i.e., when the basicity of slag is 3, $w(Al_2O_3)$ is controlled within 2.72% and the oxygen content in the steel is less than 2.89×10^{-4} wt.%.
2. The developed deoxidation kinetic mass transfer model was validated by laboratory data to be suitable for studying the deoxidation behavior of CaF_2–CaO–Al_2O_3–MgO–SiO_2-type slag with different R, Al_2O_3 and CaF_2 contents in SS-5Si. The RCS of the deoxidation reaction was confirmed by the reaction maximum rate equations to be the mass transfer of O in the molten steel. The oxygen mass transfer coefficients in the molten steel varied in the range of 4.0×10^{-6}–4.3×10^{-5} m s^{-1} and became larger with increasing the basicity. However, the mass transfer coefficients were essentially the same at high slag basicity (R = 2, 3). The changes in oxygen content predicted by the mass transfer model are in good agreement with the experimental data.
3. The basicity of the slag has a great influence on the oxygen content in the steel as well as on the rate of deoxidation. The oxygen content in steel decreases with increasing basicity. When the slag composition includes 29.23 wt.% CaF_2, 44.53 wt.% CaO, 14.84 wt.% SiO_2, 9.60 wt.% MgO, and 1.80 wt.% Al_2O_3, the total oxygen content in the steel can achieve a minimum of 3.2×10^{-4} wt.%. At 1873 K, the TO content in steel decreases from 22×10^{-4} to 3.2×10^{-4} wt.%. The slag–steel deoxidation reaction takes 15 min to reach equilibrium when R = 2 (w[O] = 5.5×10^{-4} wt.%), but takes 30 min to reach

Table 6 Total oxygen content of S2 experimental ingots at different temperatures (wt.%)

Temperature	0 min	1 min	5 min	10 min	15 min	30 min
1773 K	22.0×10^{-4}	12.5×10^{-4}	8.3×10^{-4}	5.4×10^{-4}	3.2×10^{-4}	2.6×10^{-4}
1823 K	22.0×10^{-4}	13.7×10^{-4}	10.0×10^{-4}	7.3×10^{-4}	4.3×10^{-4}	3.5×10^{-4}
1873 K	22.0×10^{-4}	17.8×10^{-4}	10.5×10^{-4}	7.9×10^{-4}	6.3×10^{-4}	5.5×10^{-4}

equilibrium at $R = 3$ ($w[O] = 3.2 \times 10^{-4}$ wt.%), which doubles time of the refining reaction. From the kinetic point of view, in the smelting of SS-5Si, reasonably controlling the slag basicity at 2 not only ensures that the depth of deoxidation solves the problem of insufficient steel purity, but also shortens the smelting cycle to improve production efficiency.

Declarations

Conflict of interest The authors declare that they have no known competing financial interests or personal relationships that could have appeared to influence the work reported in this paper.

References

[1] S. Chen, T. Liang, Y. Zhou, W. Xing, C. Zheng, Y. Ma, J. Wu, G. Li, K. Liu, Acta Metall. Sin. (Engl. Lett.) 34 (2021) 649–656.
[2] S. Kubo, M. Futakawa, I. Ioka, K. Onuki, A. Yamaguchi, Int. J. Hydrogen Energy 38 (2013) 6577–6585.
[3] D.K. Louie, Handbook of sulphuric acid manufacturing, DKL Engineering, Inc., Thornhill, Ontario, Canada, 2005.
[4] Y. Sun, R.J. Hebert, M. Aindow, Mater. Des. 140 (2018) 153–162.
[5] N. Choi, K.R. Lim, Y.S. Na, U. Glatzel, J.H. Park, J. Alloy. Compd. 763 (2018) 546–557.
[6] J.H. Park, Y. Kang, Steel Res. Int. 88 (2017) 1700130.
[7] U. Zerbst, M. Madia, C. Klinger, D. Bettge, Y. Murakami, Eng. Fail. Anal. 98 (2019) 228–239.
[8] S. Zheng, C. Chen, L. Chen, Mater. Sci. Appl. 2 (2011) 917–921.
[9] M. Elboujdaini, R.W. Revie, J. Solid State Electrochem. 13 (2009) 1091–1099.
[10] I.I. Reformatskaya, I.G. Rodionova, Y.A. Beilin, L.A. Nisel'son, A.N. Podobaev, Prot. Met. 40 (2004) 447–452.
[11] T.V. Shibaeva, V.K. Laurinavichyute, G.A. Tsirlina, A.M. Arsenkin, K.V. Grigorovich, Corros. Sci. 80 (2014) 299–308.
[12] G.L. Cao, G.M. Li, S. Chen, W.S. Chang, X.Q. Chen, J. Univ. Sci. Technol. Beijing 32 (2010) 872–876.
[13] A. Ismail, N.H. Adan, Am. J. Eng. Res. 3 (2014) 64–67.
[14] D.G. Li, D.R. Chen, P. Liang, J. Alloy. Compd. 873 (2021) 159695.
[15] Y. Zhang, W. Chen, Y. Yang, A. Mclean, ISIJ Int. 57 (2017) 322–328.
[16] C. Liu, Y. Jia, L. Hao, S. Han, F. Huang, H. Yu, X. Gao, S. Ueda, S.Y. Kitamura, Metals 11 (2021) 763.
[17] Z. Liu, G. Song, Z. Deng, M. Zhu, Ironmak. Steelmak. 48 (2021) 893–900.
[18] H.Y. Tang, Y. Wang, G.H. Wu, P. Lan, J.Q. Zhang, J. Iron Steel Res. Int. 24 (2017) 879–887.
[19] C. Guo, H. Ling, L. Zhang, W. Yang, Y. Ren, H. Zhou, Metall. Res. Technol. 114 (2017) 602.
[20] J. Lei, J. Li, L. Yang, Y. Zhang, Processes 11 (2023) 763.
[21] P. Yan, X. Guo, S. Huang, J. Van Dyck, M. Guo, B. Blanpain, ISIJ Int. 53 (2013) 459–467.
[22] J.H. Park, Calphad 31 (2007) 149–154.
[23] J.S. Han, J.H. Heo, J.H. Park, Ceramics Int. 45 (2019) 10481–10491.
[24] J.S. Han, J.G. Kang, J.H. Shin, Y. Chung, J.H. Park, Ceram. Int. 44 (2018) 13197–13204.
[25] L.F. Wang, X.H. Wang, J.M. Zhang, W.J. Wang, X.J. Zhuo, Iron and Steel 39 (2004) No. 1, 21–23.
[26] D. Durinck, F. Engström, S. Arnout, J. Heulens, P.T. Jones, B. Björkman, B. Blanpain, P. Wollants, Resour. Conserv. Recycl. 52 (2008) 1121–1131.
[27] G. Dou, H. Guo, J. Guo, S. Li, Y. Yan, Z. Wang, Front. Mater. 9 (2022) 937288.
[28] J. Zhang, Computational thermodynamics of metallurgical melts and solutions, Metallurgical Industry Press, Beijing, China, 2007.
[29] H. Guo, Metallurgical physical chemistry, Metallurgical Industry Press, Beijing, China, 2013.
[30] C. Wagner, J.F. Elliott, The physical chemistry of steelmaking, Wiley, New York, USA, 1958.
[31] W.E. Duckworth, G. Hoyle, Electroslag refining, Chapman and Hall, London, UK, 1969.
[32] R.J. Pomfret, P. Grieveson, Can. Metall. Quart. 22 (1983) 287–299.
[33] A. Podder, K.S. Coley, A.B. Phillion, Steel Res. Int. 93 (2022) 2100831.
[34] J.H. Shin, Y. Chung, J.H. Park, Metall. Mater. Trans. B 48 (2017) 46–59.
[35] Y. Ren, L.F. Zhang, Y. Zhang, J. Iron Steel Res. Int. 25 (2018) 146–156.
[36] D.C. Park, I.H. Jung, P.C.H. Rhee, H.G. Lee, ISIJ Int. 44 (2004) 1669–1678.
[37] S.Y. Li, B. Li, S.C. Duan, X.M. Zhao, J. Guo, H.J. Guo, J. Cent. South Univ. 28 (2021) 370–385.
[38] H. Suito, R. Inoue, ISIJ Int. 36 (1996) 528–536.
[39] G. Okuyama, K. Yamaguchi, S. Takeuchi, K.I. Sorimachi, ISIJ Int. 40 (2000) 121–128.
[40] Y. Ren, L. Zhang, W. Fang, S. Shao, J. Yang, W. Mao, Metall. Mater. Trans. B 47 (2016) 1024–1034.
[41] Q. Wang, L. Wang, J. Zhai, J. Li, K.C. Chou, Metall. Mater. Trans. B 48 (2017) 564–572.
[42] S. Duan, T. Kim, J. Cho, J.H. Park, J. Mater. Res. Technol. 24 (2023) 5156–5176 .
[43] M. Valdez, G.S. Shannon, S. Sridhar, ISIJ Int. 46 (2006) 450–457.
[44] J.S. Park, J.H. Park, Metall. Mater. Trans. B 47 (2016) 3225–3230.
[45] R.S.E. Schneider, M. Molnar, G. Klösch, C. Schüller, J. Fasching, Steel Res. Int. 91 (2020) 2000241.
[46] S. Zhang, H. Li, M. Ran, Z. Jiang, L. Zheng, H. Feng, J. Yu, Y. Dai, ISIJ Int. 62 (2022) 2207–2216.
[47] Z. Chen, H. Wang, Y. Sun, L. Liu, X. Wang, Metall. Mater. Trans. B 50 (2019) 2930–2941.
[48] L. Zheng, H. Li, X. Wang, Z. Jiang, H. Feng, ISIJ Int. 61 (2021) 1784–1793.
[49] S.C. Duan, X. Shi, M.C. Zhang, B. Li, W.S. Yang, F. Wang, H.J. Guo, J. Guo, Metall. Mater. Trans. B 51 (2020) 353–364.
[50] J.H. Park, K.Y. Ko, T.S. Kim, Metall. Mater. Trans. B 46 (2015) 741–748.